Full Paper

Wiley Online Library

ELECTROANALYSIS

DOI: 10.1002/elan.202060374

Application of MWCNT/Ag-Pt Nanocomposite Modified GCE for the Detection of Nevirapine in Pharmaceutical Formulation and Biological Samples

Fredrick O. Okumu,[a] Bongiwe Silwana,[a] and Mangaka C. Matoetoe*[a]

Celebrating the 65th Birthday of Prof Emmanuel I. Iwuoha: Electrochemistry in Africa

Abstract: A study of nanosensor comprising of a glassy carbon electrode modified with a composite of multiwall carbon nanotube (MWCNT) and bimetallic (Ag-PtNPs) for the determination of Nevirapine. The GCE/MWCNT/Ag-PtNPs sensor had remarkable electrocatalytic properties with enhanced response towards Nevirapine under optimized conditions. The platform electrochemical characterisation in 0.01 M NaOH solution, with cyclic voltammetry (CV), electrochemical impedance spectroscopy (EIS) and differential pulse voltammetry (DPV) is detailed. The limit of the detection (LOD) was 0.021 μM. The nanosensor was validated for real sample study using spiked pharmaceutical dose form, milk and urine samples, which showed acceptable recoveries (90- 112 %), good precision (RSD = 3.3 %, N = 3), reproducibility (RSD = 4.3 %) and excellent selectivity towards Nevirapine from studied interferents.

Keywords: electrochemical · bimetallic · nanoparticles · nevirapine · silver · platinum

1 Introduction

The analysis of active ingredients and their metabolites in biological fluids is vital in pharmaceutical and medical science [Gupta et al., 2013]. Human deficiency virus (HIV) targets and alters the immune system, increasing the risk and impact of other infections and diseases. HIV remains one of the most common infectious disease of a major public health concern. Nevirapine (11Cyclopropyl-4-methyl-5, 11hydro-6H-diprido)[3,2-b:2',3'-e][1,4] diazepin-6-one (Scheme 1) is a non- nucleoside reverse transcriptase inhibitor widely recommended for the treatment and management of infection by retroviruses, primarily HIV that can lead to acquired immune deficiency syndrome (AIDS) [Zhang et al., 2013; Chen et al, 2010, Shahrokhian et al, 2015]. Nevertheless, continuous intake of anti HIV drugs causes severe side effects. Notably, the HIV drugs are practically used in high doses for a life time. Thus, continuous monitoring of pharmaceutical dosages quality is crucial to reduce the risk of toxicity. The need to monitor and analyse anti-HIV drugs such as Nevirapine (NVP) has continued to be a great concern to most researchers worldwide. The most successful analysis technique requires high specificity, sub-nanograms detection limits in biological fluids and robustness. Various reported methods for NVP determination, involves use of reverse phase liquid chromatography (RP-HPLC [Kabra et al., 2009; Mohanraj et al., 2008], capillary electrophoresis [Chen et al., 2010], HPLC-UV [Marinho et al., 2014], LC–MS/MS [Zhang et al., 2010] and GC-MS [Vogel et al., 2010]. Some of these methods have low sensitivity, time consuming sample preparation and costly (equipment and

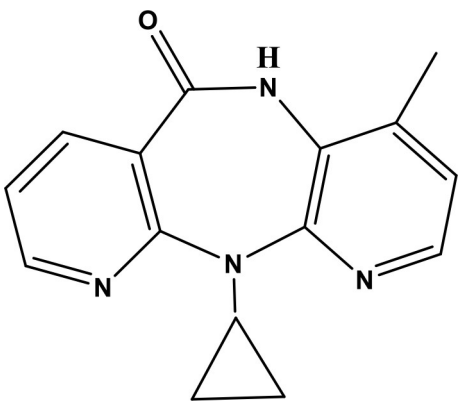

Scheme 1. Chemical structure of the investigated drug (Nevirapine).

[a] F. O. Okumu, B. Silwana, M. C. Matoetoe
Department of Chemistry,
Cape Peninsula University of Technology,
Tennant Street,
P.O. Box 652. Cape Town, South Africa
E-mail: lellangm@gmail.com

Supporting information for this article is available on the WWW under https://doi.org/10.1002/elan.202060374

analysis). Hence, it is essential to develop a method, which is less time consuming, cheaper and environmental friendly.

Electrochemical techniques have been utilised in analyses of various drug molecules since they offer very low detection limits for electroactive molecules [Castro et al., 2013; Dogan et al., 2008]. Various electrodes were used to detect Nevirapine and the mechanism of reaction proposed based on the electrode interaction with NVP as an electron transfer process [Teradal et al., 2012; Esteva et al., 2014] with an irreversible behaviour. Previous studies on the electrochemical determinations of NVP have explored bare GCE [Teradal et al., 2012], gold electrode [Esteva et al., 2014] mercury electrode [Castro et al., 2013], carbon paste electrode [Zhang et al.,2013] as various platforms of NVP detection with few done on modified electrodes.

Some of the reported modifications on electrodes for NVP detection include CuO NPs/GCE platform [Shahrokian et al., 2012]. These platforms have provided good detection probes though with challenges such as electrode fouling and low sensitivity.

Carbon based nanomaterial have been widely exploited for fabrication of electrochemical sensors on account of their low excellent corrosion resistance in various electrolytes solution [Ramachandran et al., 2016] MWCNTs have much higher stability against electromigration than other small metallic structures and therefore they find applications as possible links on modified electrodes. For example, MWCNTs have been mixed with silver [Hayos-Palacio et al., 2019] or cobalt [Shahrohian et al., 2009] nanoparticles via insitu chemical vapour deposition and to measure thioridazine, respectively. Ag–Pt bimetallic nanoparticles have been extensively studied because Ag has the highest optical cross section of any metal but it is easily oxidized while Pt is known as a catalyst for many chemical reactions. Bimetallic nanoparticles of Ag–Pt combined with CMWNTs are of particular interest due to their known properties and can be manipulated in a desirable way.

This work focuses on the application of GCE/MWCNT/Ag–Pt nanosensor for determination of NVP in pharmaceutical dosage form and biological fluids, which is a continuation of our previous work [Okumu et al., 2016]. The previous report of our study included the synthesis of Ag–Pt nanoparticles at different ratios, and the electrochemical properties of the films on GCE are detailed. As a result of the unstable signal resolutions of bimetallic Ag–Pt NPs as previous reported, MWCNT supported bimetallic Ag–Pt NPs electrode was constructed and used for the detection of NVP. This nanosensor showed superior electroanalytical behaviour attributed to an increase in surface area, presence of electronic structure and higher intrinsic electrical conductivity for the determination of NVP. To the best of our knowledge, there are no reports in the literature using MWCNT supported bimetallic nanoparticles for the electrochemical detection of NVP.

2 Experimental

2.1 Reagents and Apparatus

All reagents used were of analytical grades and used without further purification. Deionized water was used throughout the study. NVP standard was purchased from industrial Analytical South Africa. The sodium hydroxide; ethanol and MWCNT were purchased from Sigma Aldrich (S.A). The sodium hydroxide solution was used to prepare electrolytes solution.

Electrochemical measurements were performed using Autolab PGSTAT 101(Metrohm, S.A). All electrochemical measurements were carried out in a solution purged with high purity nitrogen gas at 5 min and blanketed with nitrogen atmosphere during the measurements. A conversional three electrode system consists of GCE (BASi, 3 mm in diameter and $A = 0.071\ cm^2$) was used as a working electrode, a platinum wire (3 mm) in diameters from Metrohm (S.A) as a counter electrode and a Ag/AgCl (3 M KCl) electrode from BASi was used as reference electrode. All potentials were quoted with respect to Ag/AgCl and the experiments were carried out at room temperature. The behaviour of NVP was tested in 0.01 M NaOH as the supporting electrolytes by using CV in the potential range −0.6 to 1.0 V vs Ag/AgCl at the scan rate of 20 mV/s. The DPV was used for quantitative experiments with the pulse amplitude of 0.025 V vs Ag/AgCl and the scan rate of 20 mV/s.

The ratio of voltage versus current (slope of the calibration curve) was used to measure the NVP sensitivity and the detection limit was measured (from 3 x standard deviation of blank) in the linear dynamic range of the calibration.

Electrochemical impedance spectroscope was recorded in the frequency range of 10^5 to 10–1 Hz. The X-ray diffraction (XRD) characterization of the NPs was performed using a Bruker AXS D8 Advance diffractometer with cu-Kα radiation over the scan rate range $2\Theta = 20^\circ - 90$ at a voltage of 40Kv and 40 mA

2.2 Preparation of the Modification Electrode

Ag–Pt bimetallic nanoparticles were synthesized based on our previous work [Okumu et al., 2016]. In typical synthesis process involve monometallic NPs of (Ag and Pt) [Harriman et al., 1988] and the one pot synthesis of bimetallic Ag–Pt at in ratios (Ag–Pt ratios 3:1) [Okumu et al., 2016]. As the results of the unstable bimetallic nanocomposite, MWCNT was used to support the Ag–Pt bimetallic nanoparticles. Prior to each modification, the GCE was polished repeatedly with 1, 0.3 and 0.05 μm alumina to obtain a mirror effect. After each polishing, the electrode was successively rinsed for 5 minutes with doubly distilled water, ultra-sonicate in ethanol and finally with another doubly distilled water to remove any adsorbed substances on the electrode surface, thereafter rinsed with deionized water. GCE was modified with monometallic NPs (Ag and Pt), bimetallic NPs (Ag–Pt

ratios 3:1) and MWCNT/ Ag–Pt nanocomposites via drop casting method. Then, the electrodes were left to dry at room temperature before use. The resulting electrodes were denoted as GCE/MWCNTs/AgNPs, GCE/MWCNTs/PtNPs, GCE/MWCNTs/Ag-PtNPs and GCE/MWCNTs//Ag-PtNPs. Figure 1 shows the Transmission emission spectroscope (TEM), selected area electron diffraction (SAED) pattern; 2D and 3D atomic force microscope (AFM) topographic images of AgPtNPs in a ratio 3:1 ratio.

2.3 Sample Preparation

Stock solutions of NVP were prepared in methanol to water with 80:20 % v/v solution and kept at 4 °C in the refrigerator. The working solutions of NVP were freshly diluted from their stock solution, and the 15.0 ml of NaOH solution was kept constant during measurements. Drug free milk purchased from the local shop and human urine samples were spiked with 0.76, 1.14 and 1.52 µM of NVP. The NVP tablet was crushed and soaked in methanol for 24 hours. The suspension was filtered, and the resulting solution was transferred to a 100 ml volumetric flask and completely filled up with methanol. It contained 3.57 mg ml^{-1} of NVP and the working solutions were prepared from this solution.

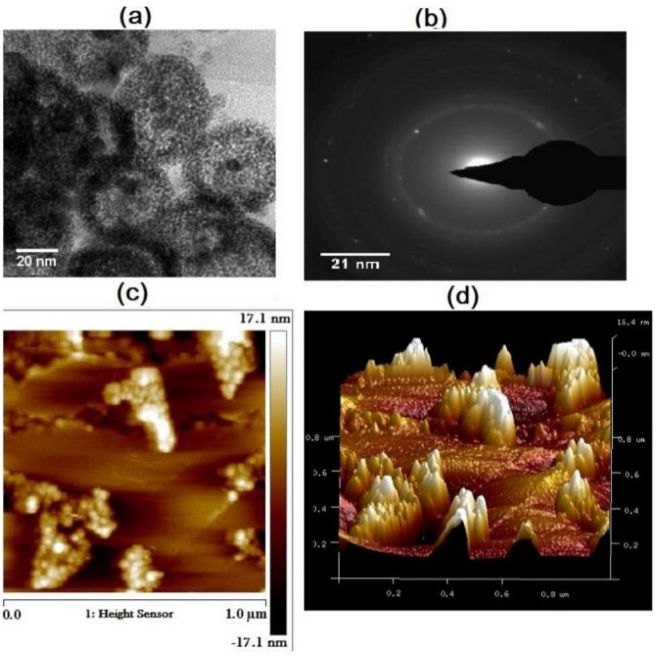

Fig. 1. Transmission electron microscope (TEM) studies of Ag–Pt bimetallic nanoparticles (AgPtNPs) morphology with 20 nm magnification. (a); Selected area electron diffraction (SAED) pattern of AgPtNPs (b); Atomic force microscope images of AgPtNPs 2-D topography (c) and 3-D topography (d).

3 Results and Discussions

3.1 Characterization of the Modified Electrodes

The electrochemical behaviour of the known amount of NVP at GCE and at the different platforms was examined in 0.01 M NaOH as supporting electrolytes by CV, DPV, EIS and XRD as seen in Figure 2, 3, 4 and 5. Figure 2 shows the CV response of 1.52 µM NVP studied in the range of −1.5 V–1.5 V vs Ag/AgCl using a bare and modified GCE. The electrochemical response of NVP on monometallic (AgNP, PtNP) was poor compared to the one supported by MWCNTs as shown in Figure S1. In the CV of GCE/AgNPs a redox pair was observed at potentials −0.028 and 0.028 V, respectively. This study is similar to the previously reported data. [Van der Horst et al., 2015]. The effect of MWCNTs was investigated using the CV in Figure 2. Accordingly, the bare GCE showed the lowest response of the NVP peak. The MWCNTs/Ag-PtNPs showed highly enhanced peak current response of NVP due to the fast electron transfer provided by nanocomposite compared to all platforms as can be seen in Figure 2.

The collective inclusion of MWCNT with bimetallic nanoparticles of Ag–Pt resulted in a better response compared to a single effect of each modifier as seen in Figure 2 and Figure S1. We speculate that the presence of the Ag–Pt bimetallic nanoparticles increases the electrode surface area due to high porosity and a good conductivity provided by MWCNTs mixed and greatly increased the current [Zhang et al., 2013]. The voltammograms showed oxidation peak (A), this peak may be related to oxidant species of the nanocomposite. The irreversible oxidation peak around 0.59 V vs Ag/AgCl corresponds to the oxidation of the NVP labelled as "NVP" in most detection platforms. These results are within the range of the work reported by Zhang and co-workers [Zhang et al., 2013]. All other peaks observed were characteristic

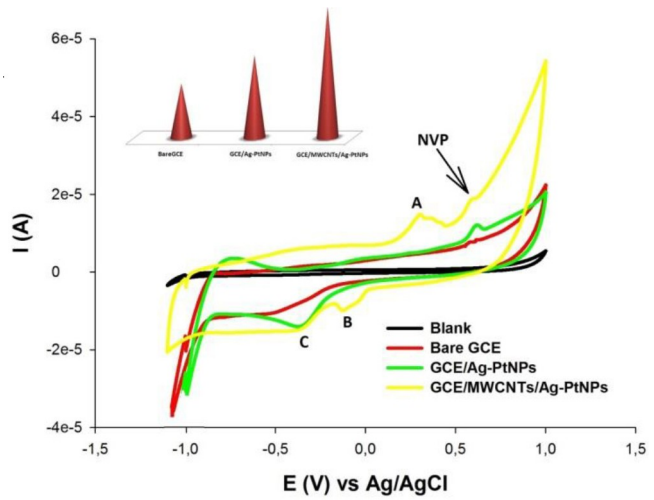

Fig. 2. Behaviour of bare GCE and various modified electrodes in 1.52 µM NVP in 0.01 M NaOH solution at scan rate 20 mV/s.

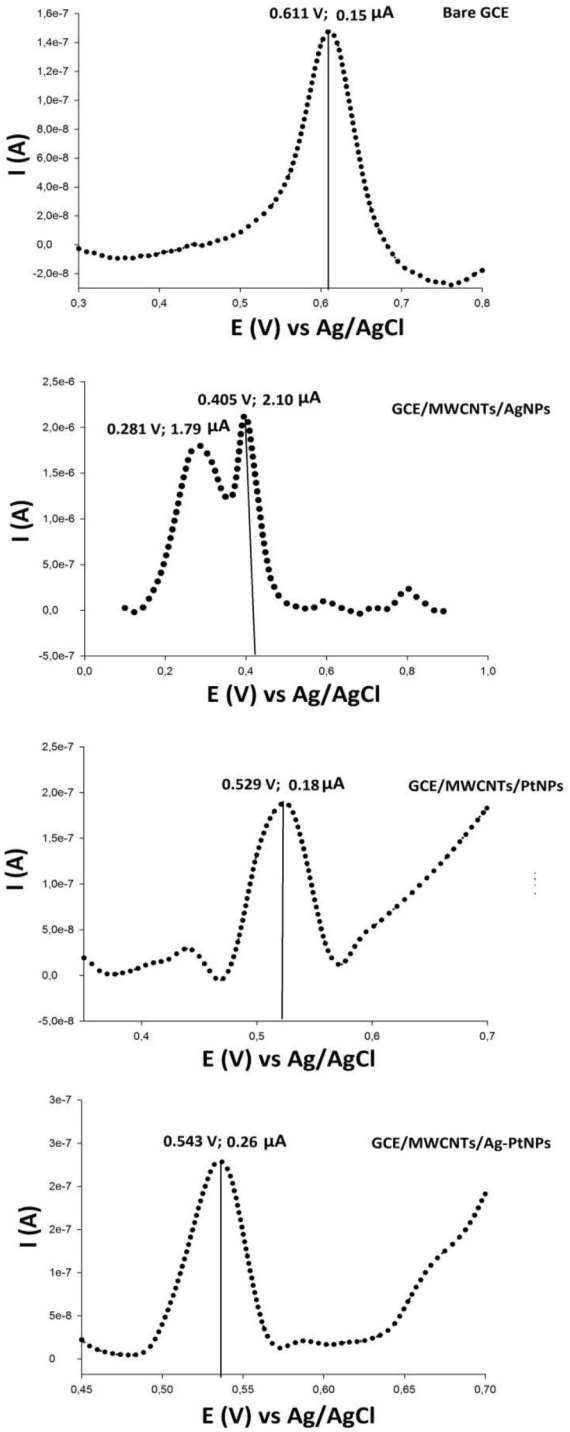

Fig. 3. Recorded DPV voltammograms of GCE, GCE/MWCNTs/AgNPs, GCE/MWCNTs/PtNPs and GCE/MWCNTs/AgPtNPs after addition of 1.52 µM NVP in 0.01 M NaOH at 20 mV/s.

of the modified electrodes previously discussed [Okumu et al., 2016] in our work. From the obtained results, it was concluded that MWCNT/Ag-PtNPs enhance the electron transfer of the analyte and the electrode thus; it would be an interesting alternative to the determination of the NVP in real samples.

Furthermore, DPV was also employed to scrutinize the electrochemical response of NVP at bare GCE and modified GCE. Figure 6 shows the voltammograms of bare GCE as well as GCE/MWCNTs/Ag-NPs, GCE/MWCNTs/PtNPs GCE/MWCNTs/Ag-PtNPs in 0.01 M NaOH solution containing 1.52 µM NVP. As shown in the voltammograms, the obtained peak potentials and current are quite distinguishable. The anodic peak current at GCE/MWCNTs/Ag-NPs was higher than those recorded with other electrodes.

The oxidation of NVP by GCE/MWCNTs/Ag-PtNPs gives rise to a single peak at 0.543 V vs Ag/AgCl and GCE/MWCNTs/AgNPs gave two peaks at 0.281 V and 0.402 V vs Ag/AgCl. The peak current in the case of GCE/MWCNTs/AgNPs is greater than GCE/MWCNTs/Ag-PtNPs; however, it is broader with two peaks formed, which makes the detection of the individual concentration of NVP complicated. From the peak analysis, this indicates that the GCE/MWCNTs/Ag-PtNPs sensor is suitable for the determination of NVP.

The interface properties of the modified electrodes and GCE were further investigated. For interface modelling, Nyquist plots along with Randle's equivalent circuit obtained using Z-view software are shown in Figure 4. The equivalent circuit consists of uncompensated solution resistance (Rs), capacitance (C) and a charge transfer resistance (Rct). At the electrode interface, the electron transfer of the redox probe is controlled by R_{ct} which is associated with the surface area and electrical conductivity [Moreira et al., 2014]. The first point in the plot is the bare GCE shown for reference.

A combination of all modifiers on GC electrodes resulted in a remarkable decrease of the charge transfer resistance (10.18 Ω) as seen in Table 1. The GCE/AgNPs,

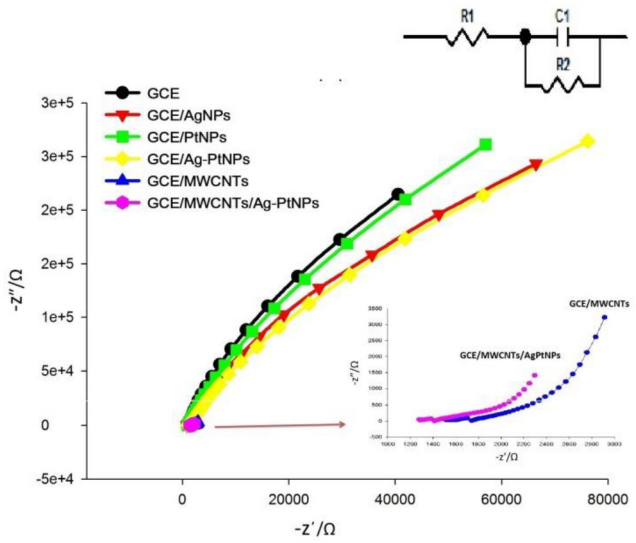

Fig. 4. Nyquist plot of bare GCE and different modified GCE (GCE/AgNPs, GCE/PtNPs, GCE/MWCNTs and GCE/MWCNTs/Ag-PtNPs. Plots were recorded in frequency range from 10^5 to 10^{-1} Hz

Table 1. Parameters employed for fitting of the EIS by use of an equivalent circuit model.

Modified Electrodes	Rs (Ω)	Rct (Ω)
GCE	46.77	19.63
GCE/AgNPs	41.42	26.00
GCE/PtNPs	49.16	14.57
GCE/Ag-PtNPs	46.64	15.66
GCE/MWCNTs	16.92	2.31
GCE/MWCNTs/Ag-PtNPs	10.18	2.62

GCE/PtNPs and GCE/Ag-PtNPs showed a weaker interfacial electron transfer compared to other electrodes. The good stability and electrical conductivity caused a decrease in the Nyquist plot of both GCE/MWCNTs and GCE/MWCNTs/Ag-PtNPs. Such properties can be considered when selecting the correct material tailor made for a specific application.

The decrease which occurs at the high frequency region indicates small interface impedance and it is associated with the interfacial charge transfer resistance of the electrode and electrolytes solution. An influential electron transfer paths between the supporting solution and the electrode surface caused the decrease. The solution resistance for both GCE/MWCNTs and GCE/MWCNTs/Ag-PtNPs was very low at 2.31 Ω and 2.62 Ω, respectively compared to other modifiers. In literature, a small value of Rs ensures good binding between electrode and the nanoparticles [Chen et al., 2015]. A smaller Rct value specifies the capability for a quicker electrocatalytic lessening of ions in the electrolytes [Mokurala et al., (2016], while the high value is due to the reduced binding strength of the modifier and the electrode.

Further confirmations of the structures at the crystallographic level, the nanoparticles were characterized by XRD. The results of XRD patterns of the monometallic silver, platinum and bimetallic Ag–Pt NPs are shown in Figure 5. For more detailed discussion on the topic of optical and morphological analysis of the bimetallic Ag-PtNPs, the reader is referred to our published paper (reference 18).

AgNPs showed distinct peaks of characteristic face centred cubic planes at 30.08° (111), 44.20°(200), 64.30° (220), 77.20° (311) and 81.6° (222). These peaks are in agreement with the studies done by Peng and co-workers [Peng et al., 2008]. Thus, it indicates the crystalline structure of AgNPs. In the case of PtNPs, multiple diffraction peaks that are clearly distinguishable formed at 2Θ values of 33.90°, 45.78°, 66.60° and 84.20° correspond to the 111, 200, 220, and 222 crystal planes of face-centred cubic structure respectively as previously reported [Jingyu et al., 2007; Yang et al., 2008]. It is worth noting that the broader peak observed at 24° 2Θ is due to the graphitic carbon used as support. The XRD of bimetallic NPs showed doubled peaks which reflect the resultant crystalline of the bimetallic NPs, which were intact throughout. The diffraction pattern of bimetallic NPs

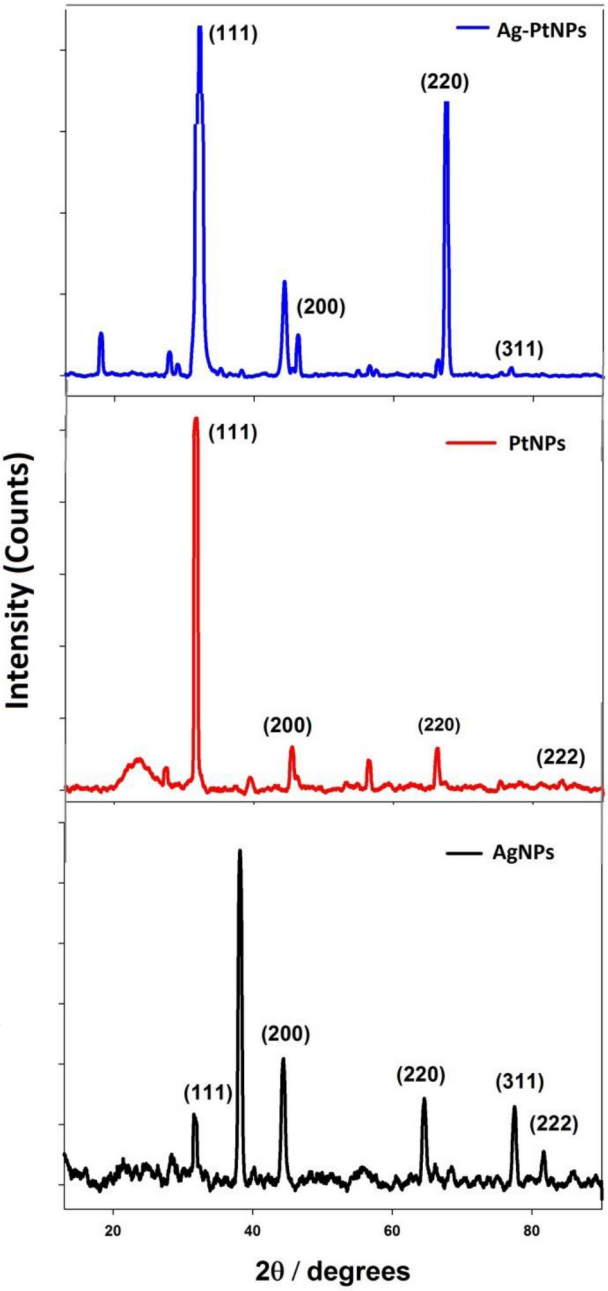

Fig. 5. XRD patterns of monometallic (AgNPs, PtNPs) and bimetallic Ag-PtNPs.

displayed mostly the reflection of characteristics of both Ag and Pt NPs and, the peaks were slightly shifted to higher 2Θ values suggesting some atomic interaction of Ag and Pt.

Conclusions supporting XRD for the presence of Ag and Pt elemental composition was confirmed by EDX and SAED, ring patterns revealed a single face centred cubic crystalline nature of AgNPs and typical Pt-based bimetallic randomly overlapping ring patterns with sharp diffraction spots [Okumo et al., 2016].

3.2 Kinetics Analysis

The effect of the scan rates on the peak current and peak potential of NVP was evaluated by varying scan rates; it is possible to outrun the chemical reaction that might happen to the electrode. The CV results demonstrated that along with the increase of the scan rate, the oxidation peak currents of NVP increased gradually. Previous results carried out in our lab have already identified the peaks shown at A, B and C [Okumo et al., 2016], the peak labelled NVP corresponds to the electro-oxidation of NVP. This behaviour is expected for the irreversible system. Diffusion coefficient of $5.20\times10^{-10}\,cm^2s^{-1}$ was obtained from a linear plot of Figure S2, where peak current varied linearly with the square root of the scan rate, indicating that the mass transfers and the electrochemical reaction of the NVP is a diffusion controlled as similarly noted [Taredal et al.,2015; Shahrokhian et al.,2009].

To evaluate the kinetics of the NVP on the GCE/MWCNT/Ag-PtNP, a plot of the logarithm peak current as the function of the oxidation peak potential is shown in Figure 6b. Figure 6b revealed a positive shift in the peak potential position (E_{pa}) with the log of scan rate (log v) for further confirming that the electro-oxidation process of NVP is irreversible. According to the method demonstrated by Laviron's equation [Laviron, 1979] for an irreversible electrode process, the oxidation peak potential (E_{pa}) is defined by the following equation,

$$E_{pa} = E^{o} + \frac{2.303RT}{\alpha nF}\log\left(\frac{RTK_S}{\alpha nF}\right) + \left(\frac{2.303RT}{\alpha nF}\right)log\vartheta\left(mVs^{-1}\right) \quad (1)$$

Where (α) is the transfer coefficient, (k) is the standard heterogeneous rate constant of the reaction, n is the number of electron transferred in the electro-oxidation of NVP, v is the scan rate, and E^0 is the formal redox potential, F is the Faraday constant, R as a universal gas constant and T as absolute temperature. Thus the value of αn was calculated from the slope of E_p versus log v using $T=298\,K$, $R=8.314\,J\,K^{-1}mol^{-1}$, and $F=96480\,C\,mol^{-1}$. A was calculated to be 0.67 and αn was found to be 1.3 with a formal potential (E^0) of 0.560. Furthermore, the value of k_s was found to be $0.884\,s^{-1}$. The obtained results are summarized and presented in Table S1. Hence, the number of electrons was found to be 2. Since the number of electrons and protons were transferred equally. Based on these results and the similarly reported [Shahrokhian et al., 2015; Zhang et al., 2013; Antunes et al., 2012], a probable electrode reaction mechanism involving two-electrons and two-protons is shown in Scheme 2.

3.3 Influence of Operation Parameters

Owing to the recognition properties of MWCNT/Ag-PtNPs, its effect as a modifying agent was investigated

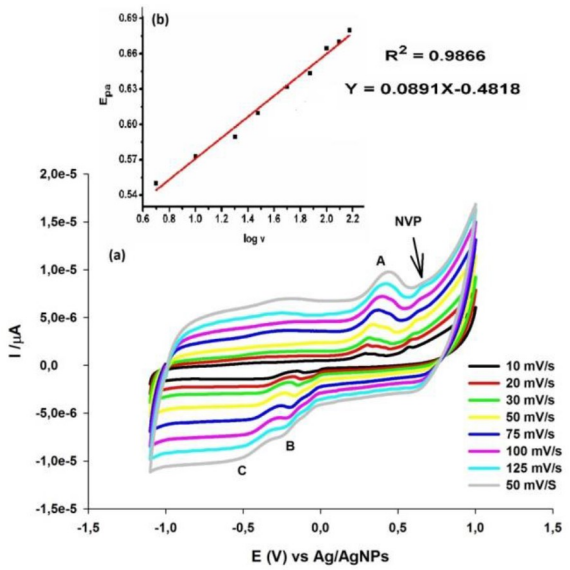

Fig. 6. CV of GCE/MWCNTs/AgPtNPs in 0.01 M NaOH containing 3.81 µM NVP at different scan rates in the range 10 to 150 mV/s (a) Inset: Laviron plot, linear relationship of anodic peak current versus log scan rate (b).

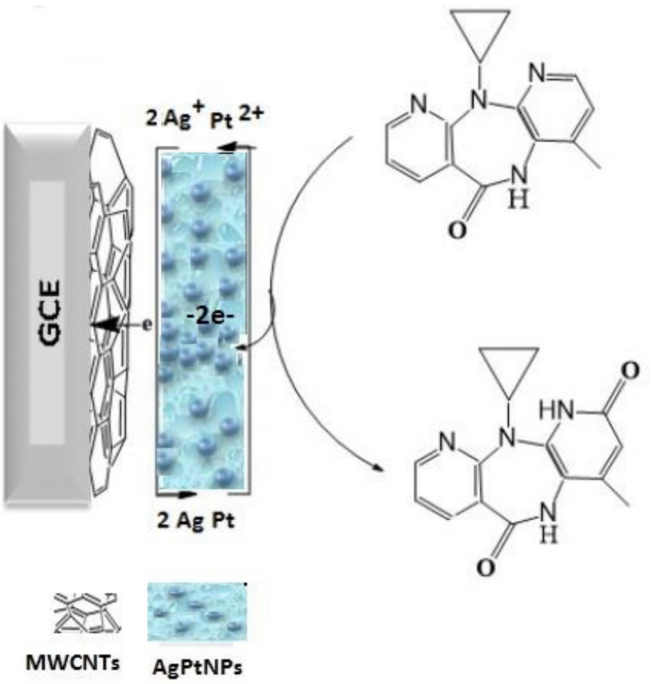

Scheme 2. The electrochemical oxidation mechanism of NVP on GCE/MWCNTs/Ag-PtNPs.

focusing on the possibility of extending its application for real samples. To achieve the best electrode configuration certain parameters were optimized. The Ag and Pt loading were investigated for the best sensor preparation (results not shown). Hence, a 3:1 ratio was selected for the NVP determination. The relationship between pulse amplitude and oxidation peak current as well as initial potential was also studied. As shown in Figure S3, the impact on varying the pulse amplitude on the voltammetric current intensity was determined over the range of 0.005-0.060 V vs Ag/AgCl and 0.025 V gave the best peak current with well resolved signals and thus was chosen for further studies. The variation in the initial potential (from −0.03 to 0.50 V) on the NVP detection was investigated (Figure S3b) with several parameters including the peak potential (Ep), and peak current (Ip) analyzed. When the initial potential of 0.20 V was used, a well-defined NVP peak (Ep) at −0.557 V (Ip = 12.87 μA) with the best background resolution was obtained. Although other initial potential ranges used showed significant peaks of NVP oxidation, they had poor resolution. From Figure S3b beyond 0.20 V, the peak current of NVP decreases with the increase in the initial potential for more positive potentials (Figure S3b). The initial potential in 0.20 V versus Ag/AgCl was therefore selected and used for further experimental measurements. The initial potential of 0.20 V vs Ag/AgCl and pulse amplitude of 0.025 V vs Ag/AgCl was the ideal choice and used for further experimental measurements.

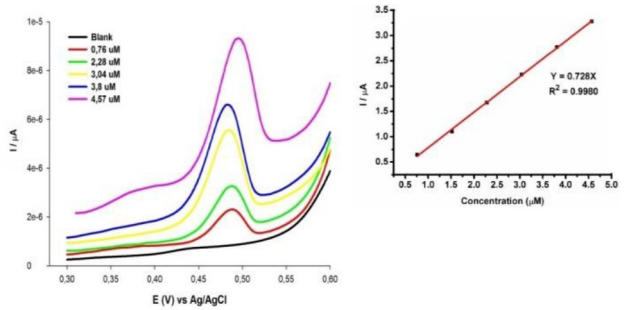

Fig. 7. DPV curves obtained in 0.01 M NaOH at scan rate 20 mV/s using the GCE/MWCNTs/Ag-PtNPs. Inset: calibration plot for various concentrations of NVP.

4 Sensor Performance and method Validation

4.1 Reproducibility, Repeatability and Stability

The efficiency of the proposed method parameters such as precision, reproducibility, stability, linearity, limit of quantification (LOQ) and limit of detection (LOD) was evaluated by DPV under optimized conditions.

Figure 7 depicts the DPV curves recorded using GCE/MWCNT/Ag-PtNPs on various concentrations (0.76–4.57 μM) of NVP in 0.01 M NaOH solutions at a potential ranging from 0.3 −0.8 V vs Ag/AgCl. The equation of the calibration curves was determined as I_{pa} (μA) = 0.728 C (R^2 = 0.9980). From the measurements, the best response with high sensitivity of 10.25 μA μM^{-1} cm^{-2} and good linearity was obtained. The LOD and LOQ were calculated as 2.10×10^{-8} and 6.98×10^{-8} mol L^{-1} respectively. The reproducibility of the bimetallic MWCNT composite nanosensor was assessed using 3.81 μM NVP by comparing the response to six electrodes independently prepared for similar experimental conditions. The relative standard deviation (RSD) value was 4.3 %. The precision was obtained by measuring the peak currents of four replicating measurements of 3.81 μM NVP solutions using the same modified electrode. The resulting RSD% value was 2.52 %, indicating an acceptable precision. The stability of MWCNT/Ag–Pt NPs 3:1/GCE was tested in the NVP solution intermittently. The oxidation current response of NVP was maintained at 86 % even after the electrode was stored dry at room temperature for 5 days. These results were compared with earlier reported electrochemical and non-electrochemical methods from the literature and were found to be lower (Table 2). This indicates that GCE modified with Ag–Pt NPs in the presence of

Table 2. Comparison of various electrochemical methods for the detection of NVP.

Method	Sensor	Linear range (μM)	LOD	Reference
DPV	GCE/MWCNTs/Ag-PtNPs	0.76–3.81	0.021	This work
DPV	Au Electrode	1.1–3.8	–	Esteva et al., 2014
DPV	Bare GCE	5.0–350	1.026	Teradal et al., 2012
DPV	Ura/CPE	0.1–70.0	0.05	Zhang et al., 2013
AdSV	HgFilm Electrode	0.04–0.5	0.003	Castr et al., 2013
LSV	GCE/CuO-CNPs	0.1–100	0.066	Shahrokian et al., 2012
DPV	CPE/Bi2O3NPs	0.05–50	0.033	Teradal et al., 2015
DPSAV	GCE/(MB)p/AuNPs	0.1–50	0.056	Haselia et al., 2015
Amperometry	GCE/MWCNTs/AgNPs-MHHC	0.05–21	0.014	Ahmadi et al., 2019
CV	GCE/Pd@rGO/MoS_2 QDs	0.1–80	0.05	Tiwari et al., 2018

[a] Limit of detection.

Table 3. Results of the analysis of NVP in milk and human urine samples (n = 3).

Sample	NVP(μM)	Recovery (μM)	%Recovery	%RSD
Milk	0.76	0.86	112.04 ± 0.4	3.89
(From local shop)	1.14	1.05	92.04 ± 0.9	1.08
	152	1.37	90.23 ± 0.8	1.16
Human urine	0.76	0.82	108.89 ± 2.3	1.95
	1.14	1.15	99.87 ± 0.9	1.87
	1.52	1.45	96.05 ± 2.9	3.04

MWCNT has satisfactory results and can be used for the detection of NVP.

4.2 Interferences Studies

Under the optimized conditions, the influence of different interference in the detection of the NVP were investigated in 0.01 M NaOH solutions containing 0.76 μM of the NVP. The experimental results showed a significantly little effect on the current response of NVP even in the presence of 5-fold and 10-fold excess concentration of sodium chloride (NaCl), calcium chloride ($CaCl_2$) and ascorbic acid (AA). The interference were chosen based on their point sources such as food supplements ($CaCl_2$), liquid drips (NaCl) and vitamin supplements (AA), which are commonly within reach of HIV patients. As shown in Figure S4, the proposed bimetallic nanosensor exhibited excellent selectivity to NVP in the presence of several other compounds that may be present in clinical samples. It could be applied for the determination of NVP in pharmaceutical and biological samples.

4.3 Analysis of Milk and Human Urine

The developed bimetallic MWCNT composite nanosensor method was validated according to technical reports of the World Health Organisation. GCE/MWCNT/Ag–Pt NPs was used for the direct determination of NVP in milk and human urine samples. In addition, the accuracy of the method was tested by spiking the real samples with different amounts of standard NVP solutions. For this experiment, drug free milk samples and drug free urine samples were spiked with 0.76, 1.14 and 1.52 μM of NVP and the DPVs were then recorded to calculate the recovery values. The results are summarized in Table 3.

The percent recoveries of NVP were determined by comparing the peak currents of the drug in urine and milk samples with those of pure NVP using the calibration curve. The recovery range of NVP was obtained between 90 % and 113 %. This shows that the proposed method is readily acceptable to analytical applications.

4.4 Analysis of Pharmaceutical Tablets of Nevirapine

The practical analytical application of the developed method was further established by determining NVP concentrations of commercial tablets (each tablet contains 200 mg from Aspen, South Africa). Figure 8 shows the DPV of the standard addition of NVP. Three standard additions were used, 2.5, 10 and 15 μL on 0.76 μM NVP equivalent to 1.14, 2.28 and 3.04 μM respectively. Increasing the concentration of NVP increases the anodic peak response of NVP.

There were good recoveries obtained as indicated in table 4. The tablet active ingredient was found to be around 195 and 198 mg per tablet using a direct calibration graph and standard addition method, respectively.

5 Conclusion

In summary, a sensitive sensor based on MWCNT/Ag–Pt composite modified GCE was developed for the determination of NVP. The results discussed above demonstrate that the sensor resulted in an improvement on the

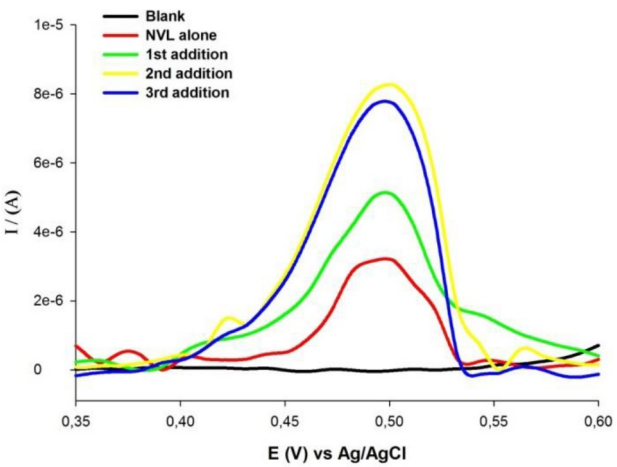

Fig. 8. DPV plots for increasing standard addition of NVP tablet in 001 M NaOH at scan rate of 20 mV/s.

Table 4. Determination of NVP in pharmaceutical tablet (Aspen Nevirapine, 200 mg).

Standard addition of NVP tablet to NVP	NVP: 5	NVP: 10	NVP: 15
Concentration1	1.26	2.12	2.80
% Recovery	109.2 ± 2.7	92.8 ± 1.1	93.1 ± 0.9
% RSD[a]	4.07	1.43	1.38

[a] Relative standard deviation.

electron transfer, enhancement of the oxidation peak current of NVP, and the decrease in the oxidation overpotential relative to other detection platforms, indicating efficient catalytic activity in the detection of NVP. In addition, the electrochemical sensor showed some clear advantages under optimized conditions such as very low detection limit, good stability, favourable reproducibility and simply preparation method. This work illustrates that the modified bimetallic nanosensor can provide a rapid and convenient method. Thus, it is a potential candidate for electrochemical determination of NVP in related drugs as well as active biological samples.

Acknowledgements

The authors acknowledge the assistance of the NRF grant (NRF unrated) and CPUT in carrying out the Study. The authors involved declare that they are no conflict of interest with any institution on this publication

Data Availability Statement

The Data in this publication can be accessed through the corresponding author.

References

[1] A. K. Gupta, R. S. Dubey, J. K. Malik, *Int. J. Pharm. Sci. Res. IJPSR* **2013**, *4*, 2450–2458.
[2] F. Zhang, L. Li, L. Luo, Y. Ding, X. Liu, *J. Appl. Electrochem.* **2013**, *43*, 263–269.
[3] J. Chen, J. Shao, R. Cai, Y. Shen, R. Zhang, L. Liu, T. Qi, H. Lu, *PLoS One* **2014**, *9*, 3–10.
[4] S. Shahrokhian, R. Kohansal, M. Ghalkhani, M. K. Amini, *Electroanalysis* **2015**, *27*, 1989–1997.
[5] V. Kabra, V. Agrahari, C. Karthikeyan, P. Trivedi, *Trop. J. Pharm. Res.* **2009**, *8*, 79–86.
[6] P. Mohanraj, D. K. Sarkar, T. Choudhury, K. Gauthaman, *E-Journal Chem.* **2008**, *5*, 1081–1086.
[7] W. Chen, W. Li, X. Ling, X. Wang, J. Liu, *J. Chromatogr. B Anal. Technol. Biomed. Life Sci.* **2010**, *878*, 1714–1717.
[8] A. T. Marinho, A. L. A. Godinho, D. A. Novais, A. M. M. Antunes, M. M. Marques, T. Ramos, C. G. Dias, E. C. Monteiro, S. A. Pereira, *Anal. Methods* **2014**, *6*, 1575–1580.
[9] L. Zhang, Y. Yao, J. Sun, J. Chen, X. Jia, *Pharm. Anal. Acta* **2010**, *01*, 1–6.
[10] M. Vogel, N. Bertram, J. C. Wasmuth, J. Emmelkamp, J. K. Rockstroh, C. Reichel, *J. Chromatogr. Sci.* **2010**, *48*, 91–94.
[11] A. A. Castro, A. I. P. Cordoves, P. A. M. Farias, *Anal. Chem. Insights* **2013**, *8*, 21–28.
[12] B. Dogan, B. Uslu, S. A. Ozkan, P. Zuman, *Anal. Chem.* **2008**, *80*, 209–216.
[13] N. L. Teradal, S. N. Prashanth, J. Seetharamappa, *J. Electrochem. Sci. Eng.* **2012**, *2*, 67–75.
[14] A. M. Esteva, E. Blanco, J. J. Pina, A. I. Balbin, C. Quintana, P. Hernandez, *J. Electrochem. Sci. Eng.* **2014**, *4*, 37–44.
[15] K. Ramachandran, T. Raj Kumar, K. J. Babu, G. Gnana Kumar, *Sci. Rep.* **2016**, *6*, 1–12.
[16] L. M. Hoyos-Palacio, D. P. Cuesta Castro, I. C. Ortiz-Trujillo, L. E. Botero Palacio, B. J. Galeano Upegui, N. J. Escobar Mora, J. A. Carlos Cornelio, *J. Mater. Res. Technol.* **2019**, *8*, 5893–5898.
[17] S. Shahrokhian, M. Ghalkhani, M. Adeli, M. K. Amini, *Biosens. Bioelectron.* **2009**, *24*, 3235–3241.
[18] F. Okumu, M. Matoetoe, *Acta. Metalla Sin-Engl.* **2016**, *29*, 320–325.
[19] A. Harriman, G. R. Millward, P. Neta, M. C. Richoux, J. M. Thomas, *J. Phys. Chem.* **1988**, *92*, 1286–1290.
[20] C. Van der Horst, B. Silwana, E. Iwuoha, V. Somerset, *Anal. Lett.* **2015**, *48*, DOI 10.1080/00032719.2014.979357.
[21] F. Okumu, M. Matoetoe, *J. Nano Res.* **2016**, *44*, 114–125.
[22] A. P. De Assis, L. L. Okumura, A. A. Saczk, M. F. De Oliveira, *J. Braz. Chem. Soc.* **2014**, *25*, 27–35.
[23] F. T. C. Moreira, R. A. F. Dutra, J. P. C. Noronha, M. G. F. Sales, *Procedia Eng.* **2012**, *47*, 865–868.
[24] S. Chen, A. Xu, J. Tao, H. Tao, Y. Shen, L. Zhu, J. Jiang, T. Wang, L. Pan *ACS. Sustain. Chem. Eng.* **2015**, *3*, 2652–9.
[25] K. Mokurula, S. Mallick, P. Bargava, *J. Power Sources.* **2016**, *305*, 134–43.
[26] Z. Peng, H. Yang, *J. Solid State Chem.* **2008**, 181, 1546–1551.
[27] S. Jingyu, H. Jianshu, C. Yanxia, Z. Xiaogang, *Int. J. Electrchem. Sci.* **2007**, *2*, 64–71.
[28] S. Yang, Z. Peng, H. Yang, *Adv. Funct. Mater.* **2008**, 2745–2753.
[29] E. Laviron, *J. Electroanal. Chem.* **1979**, *101*, 19–28.
[30] A. M. M. Antunes, M. Sidarus, D. A. Novais, S. G. Harjivan, P. P. Santos, J. L. Ferreira Da Silva, F. A. Beland, M. M. Marques, *Molecules* **2012**, *17*, 2616–2627.
[31] N. L. Teradal, J. Seetharamappa, *Electroanalysis* **2015**, *27*, 2007–2016.
[32] M. Haseliah, N. Hanghnazari, *Electrochem Soc. of Iran* conference **2015**, *11*, 352–353.
[33] E. Ahmadi, M. R. Eyvani, V. Riahifar, H. Momeneh, C. Karami, *Microchem. J.* **2019**, *146*, 1218–1226.
[34] P. Tiwari, N. R. Nirala, R. Prakash, *ChemistrySelect* **2018**, *3*, 5341–5347.

Received: October 12, 2020
Accepted: October 13, 2020
Published online on October 27, 2020

